

# Analog Gain Optimization in Rolling Shutter Optical Camera Communications

Vicente Matus  
*IDeTIC-ULPGC,*

Las Palmas de Gran Canaria, Spain  
vmatus@idetic.eu

Victor Guerra  
*IDeTIC-ULPGC,*

Las Palmas de Gran Canaria, Spain  
vguerra@idetic.eu

Cristo Jurado-Verdu  
*IDeTIC-ULPGC,*

Las Palmas de Gran Canaria, Spain  
cjurado@idetic.eu

Shivani Rajendra Teli  
*Czech Technical University*  
Prague, Czech Republic  
telishiv@fel.cvut.cz

Stanislav Zvanovec  
*Czech Technical University*  
Prague, Czech Republic  
xzvanove@fel.cvut.cz

Jose Rabadan  
*IDeTIC-ULPGC,*  
Las Palmas de Gran Canaria, Spain  
jrabadan@idetic.eu

Rafael Perez-Jimenez  
*IDeTIC-ULPGC,*

Las Palmas de Gran Canaria, Spain  
rperez@idetic.eu

**Abstract**—When Optical Camera Communication (OCC) systems are operated in outdoor conditions, low signal qualities constraint their feasibility due to the presence of noise and interference sources, and to the optical attenuation induced by atmospheric conditions. OCC receivers in these scenarios are prone to be affected by the quantization noise at the pixel’s analog-to-digital converter (ADC). In this paper, a strategy for optimizing the analog gain of the camera is shown. By estimating the received signal quality using the correlation coefficient, the analog gain can be maximized bellow saturation of the ADC.

**Index Terms**—Optical Camera Communications, analog gain, Pearson’s correlation coefficient.

## I. INTRODUCTION

Optical Camera Communication (OCC) is a group of schemes within the Visible Light Communication (VLC) field to be included in the IEEE 802.15.7r1 [1], and where the main principle is to use a digital camera as a receiver ( $R_x$ ), taking advantage of the low price of these devices. In OCC, the extensive use of Rolling Shutter (RS) cameras is based on their ability to scan lines of pixels delayed between each other by orders of tens of  $\mu s$  [2]. These cameras are the most available in commercial devices using Complementary Metal-Oxide-Semiconductor (CMOS) sensors [3], [4]. The signal coming from a Light Emitting Diode (LED) transmitter ( $T_x$ ) is captured by the lines of the sensor at different times, allowing the to decode several symbols from each image frame.

Outdoor applications of OCC such as localization, Vehicular VLC, and Sensor Networks, face relevant challenges such as long link spans, optical degradation by atmospheric conditions [5], and require mobility support in most cases. Applications

This project has received funding from the European Union’s Horizon 2020 research and innovation programme under the Marie Skłodowska-Curie grant agreement No 764461.

such as VLC positioning specifically rely on beacon signals, and most systems use packet structures with well-known patterns for the detection of Region of Interest (ROI) and synchronization. Correlators can be used for the recognition of such patterns [6].

The signal-to-noise ratio (SNR) at the receiver is crucial for allowing any communication link to have longer spans. The SNR depends on the transmitted power, on the attenuation factor of the channel, and in the case of OCC, it also depends on the optical lens array of the camera. In addition, various sources of noise and interference can be present. The area of the transmitter projected over the imaging sensor is also relevant in OCC, the maximum link distance is then bounded by the amount of sensor rows covered by the transmitter, in the case of RS-OCC. Geometrical derivations can estimate the image projected area [7].

In this work, the use of an analog gain control algorithm for optimizing the SNR through a cost function based on the correlation is proposed. The correlation is extensively used for spatial synchronization and channel estimation in OCC. Therefore, the inclusion of this control algorithm will have little or no impact on computation performance of the  $R_x$  if the correlation is considered already a process of other algorithms. Several experiments involving different input powers, the algorithm’s convergence iteration, and the SNR improvement are also provided.

The structure of this paper is the following. The OCC channel of an RS-based OCC system is modelled in II. The control algorithm for the optimization of the signal quality is derived in Section III. Both methodology and experimental design are described in Section IV. In Section V, the results obtained from the experiments are discussed. Finally, the conclusions of this work are drawn in Section VI.

## II. OCC CHANNEL

The simplified diagram of an outdoor OCC scenario is shown in Fig. 1 in which a VLC transmitter using On-Off Keying (OOK) modulation sends pulses of each of the red-green-blue (RGB) colors. The shape of the ROI or the pixels of the frame that are exposed to the transmitted signal is not necessarily known beforehand. The attenuation of some atmospheric conditions that might be present, *e.g.* in foggy weather, is modeled by  $A$  in dB/m. The link span  $d$  in m depends on the relative position of the source with respect to the camera and its orientation, which in most cases are constantly changing.

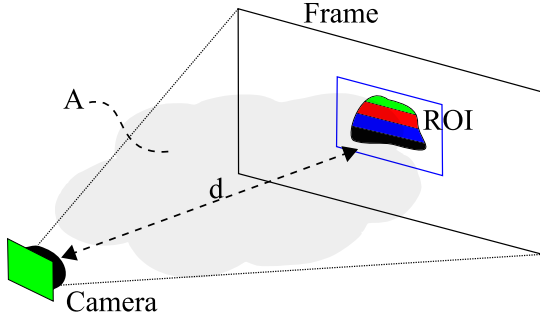


Fig. 1. Simplified diagram of the RS-OCC system considered.

The power signal at the receiver  $P_{Rx}(t)$  under an attenuated channel, when the transmitter is modeled as an  $m$ -order Lambertian source with power  $P_{Tx}(t)$ , can be expressed as

$$P_{Rx}(t) = P_{Tx}(t)e^{-Ad} \cdot \frac{m+1}{2\pi} \cdot \cos^m \theta \frac{A_{lens} \cos \Psi}{d^2}, \quad (1)$$

where  $\theta$  is the emission angle,  $\Psi$  is the incident angle, and  $A_{lens}$  is the area of the camera's external lens. From this expression, it can be seen that by varying either the transmitted power or the factor  $A \cdot d$ , known as the optical density, the received power can be affected alternatively, allowing to emulate the effect of the other parameters. Note that the projected area of the source over the camera sensor is mostly only dependent on  $d$ .

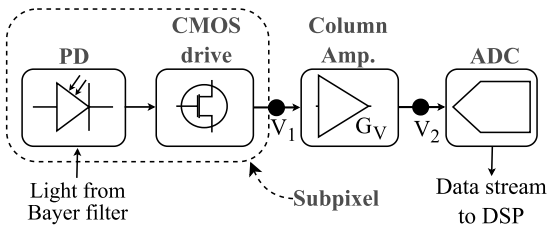


Fig. 2. Typical configuration of Complementary Metal-Oxide-Semiconductor (CMOS) camera sub-pixels.

In Fig. 2, the block diagram of a regular CMOS camera sub-pixel is shown, as described in [8]. The photodiode (PD) at position  $x, y$  and channel  $c \in \{R, G, B\}$  receives light from a colored Bayer filter and generates a current  $i_{pd}(x, y, c)$  which is turned into a voltage signal  $V_1$  by the CMOS drive. Since the

sequential reading by rows allows it, an analog amplifier and analog-to-digital converter (ADC) are shared by each column of sub-pixels of the sensor. The gain of the analog amplifiers  $G_V$  is set globally by the software of the camera and the voltage signal that is sampled by the ADC is given by  $V_2 = G_V \cdot V_1$ . The ADC induces a noise ( $\sigma_{adc}^2$ ), that can be modeled as a random Normal of mean zero with a variance that depends on the digitalization levels. The SNR of the signal that enters the digital signal processing (DSP) block can be modeled as

$$SNR \approx \frac{G_V^2 \cdot i_{pd}^2(x, y, c)}{G_V^2 (\sigma_{th}^2 + \sigma_{sh}^2) + \sigma_{adc}^2}, \quad (2)$$

where  $\sigma_{th}^2$  and  $\sigma_{sh}^2$  correspond to the thermal noise and shot noise of the process, respectively. Note that the noise induced by the ADC can be virtually reduced to zero by increasing  $G_V$  as

$$SNR \xrightarrow{G_V \rightarrow \infty} \frac{i_{pd}^2(x, y, c)}{\sigma_{th}^2 + \sigma_{sh}^2}, \quad (3)$$

nevertheless, the ADC has an upper bound for the input voltage, then  $G_V$  can only be increased up to the point  $V_2$  does not saturate the ADC.

In previous work [9], it was shown that the SNR can be obtained empirically from image frames. Nevertheless, its computation can be substituted by the calculation of the Pearson's correlation coefficient  $r_{xy}$  between the image frames and a well known template, which is used in some implementations of OCC for synchronization of the received signal in the images and also for ROI detection. The parameter  $r_{xy}$  is defined as

$$r_{xy} = \frac{\sum_{i=1}^N (x_i - \bar{x})(y_i - \bar{y})}{\sqrt{\sum_{i=1}^N (x_i - \bar{x})^2} \sqrt{\sum_{i=1}^N (y_i - \bar{y})^2}}, \quad (4)$$

where  $x_i$  are the rows of the template of size  $N$  rows,  $y_i$  are  $N$  consecutive rows of the image, and  $\bar{x}, \bar{y}$  are the mean values. The computation is iterated for all possible subsets  $y_j, y_{j+1}, \dots, y_{j+N-1}, (j + N - 1) < M$  of consecutive rows of the frame. When the template is matched in phase with the signal it emulates, the maximum value  $r_{xy}^{max}$  is achieved. This value is considered the overall correlation between the image frame and the template, which has been shown to be closely related to the SNR, giving high values of  $r_{xy}^{max}$  when the signal quality is high [9].

## III. ANALOG GAIN CONTROL ALGORITHM

As it was aforementioned,  $r_{xy}^{max}$  is closely related to SNR, and may serve as a fast estimator of it. Therefore, optimizing the correlation using  $G_V$  would implicitly maximize SNR. The following paragraphs describe each one of the development of the algorithm for controlling  $G_V$  to maximize  $r_{xy}^{max}$  proposed in this work, which is based on the typical feedback-based design, as shown in Fig. 3.

The set point  $r_{xy}^*$  is the desired value for  $r_{xy}^{max}$  to be achieved by the controller, which is set to 1 in order to force the system to get the highest signal quality.

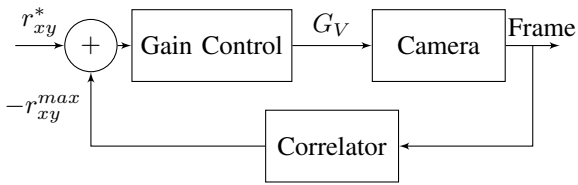


Fig. 3. Block diagram of the gain control algorithm.

The camera block receives each updated value of  $G_V$  and sets this parameter on the physical device. Generally, camera's do not have a continuum of analog gains, but a discrete range of possible values. In this work, since Sony IMX219 [10] image sensor is considered, the possible gains in linear units is defined by

$$G_V(X) = \frac{256}{256 - X}, \quad (5)$$

where  $X$  is an integer between 0 and 232 (233 possible analog gains). Due to the hyperbolic nature of  $G_V(X)$ , there is higher resolution at lower gain values. Furthermore, this quantization could be considered as an extra noise term, since each iteration will probably not coincide with valid values.

Finally, this block also captures the image and passes it to the correlation calculation block, which carries out Pearson's correlation coefficient with a parametric template. The maximum value of this operation is then forwarded to the gain control algorithm.

Mathematically, it is straightforward to define a cost function  $C(G_V)$  that optimizes  $r_{xy}^{max}$  as

$$C(G_V) = (1 - r_{xy}^{max})^2. \quad (6)$$

The performance of the control algorithm would significantly depend on the shape of the error curve. Nonetheless, in this work a simple squared difference scheme is proposed.

$C(G_V)$  can be easily optimized using an iterative approach via a gradient descent on  $G_V$ , yielding

$$G_V^{(i+1)} = G_V^{(i)} - \lambda \frac{C(G_V^{(i)})}{\partial C(G_V) / \partial G_V |_{G_V^{(i)}}}, \quad (7)$$

where  $\lambda$  is the learning rate or damping coefficient. It can be observed that the cost function's derivative can be reformulated as

$$\frac{\partial C(G_V)}{\partial G_V} = -2(1 - r_{xy}^{max}) \frac{\partial r_{xy}^{max}}{\partial G_V}. \quad (8)$$

Since there is no closed-form relationship between the correlation and the analog gain, its derivative must be numerically estimated. In this work, a  $N$ -points linear regression was performed to obtain the curve's slope on the point of interest. However, the neighbourhood of the starting point must be explored during the algorithm's initialization. This was carried out by forcing a fixed analog gain change until the estimation buffer was full to begin with the linear regressions.

Finally, combining equations 7 and 8, it yields the final iterative scheme, expressed as

$$G_V^{(i+1)} = G_V^{(i)} + \frac{\lambda}{2} \frac{1 - r_{xy}^{max(i)}}{\partial r_{xy}^{max} / \partial G_V |_{G_V^{(i)}}}. \quad (9)$$

The performance of the proposed algorithm would highly depend on the estimation of  $r_{xy}^{max}$ 's slope. As it was commented, this magnitude will be calculated using a linear regression of  $N$  points. Hence, the accuracy of Equation 9's denominator depends on the curve's shape, which will not be linear *a priori*, and the separation between samples.

#### IV. METHODOLOGY

It has been shown that the Pearson's correlation coefficient is a computationally quick estimator of the signal quality. Moreover, the camera analog gain can optimize the SNR by reducing quantization noise. The objective of this work is to propose a control algorithm for  $G_V$  based on the  $r_{xy}$  values obtained from each image capture.

In order to demonstrate this hypothesis, a series of experiments were carried out using the experimental setup shown in Fig. 4. The scenario comprises a commercial RGB lamp controlled by a general purpose microcontroller [11] and a receiver built using an Element14 Raspberry Pi board with a camera based on Sony IMX sensor [10].

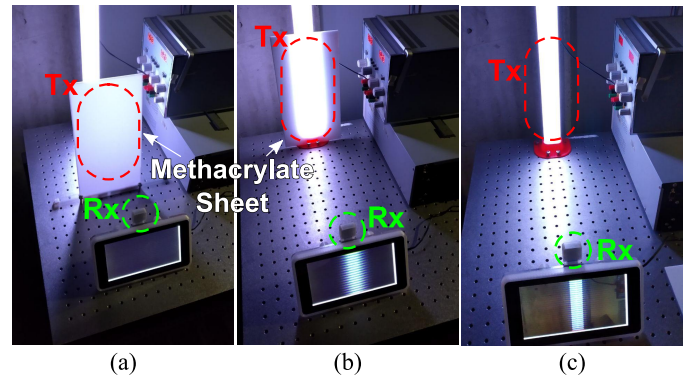


Fig. 4. Pictures of the experimental setup. In the experiments, the radiant energy at the camera position is  $3.39 \mu\text{W}/\text{cm}^2$  in (a),  $11.79 \mu\text{W}/\text{cm}^2$  in (b), and  $45.11 \mu\text{W}/\text{cm}^2$  in (c)

Three different received power levels were obtained using a Methacrylate sheet in order to emulate channel loss (optical density). All the parameters of the experiments can be observed in Table I.

The algorithm presented in Section III was evaluated for the three synthetic scenarios using different initial gain values ( $G_V^{(0)}$ ). Furthermore, the estimation of the correlation's slope was based on  $N = 4$  samples. The analyzed performance metric of the algorithms was the convergence iteration, estimated using Equation 10.

$$r_{th} = r_{xy}^{max(\infty)} (1 \pm \varepsilon) \quad (10)$$

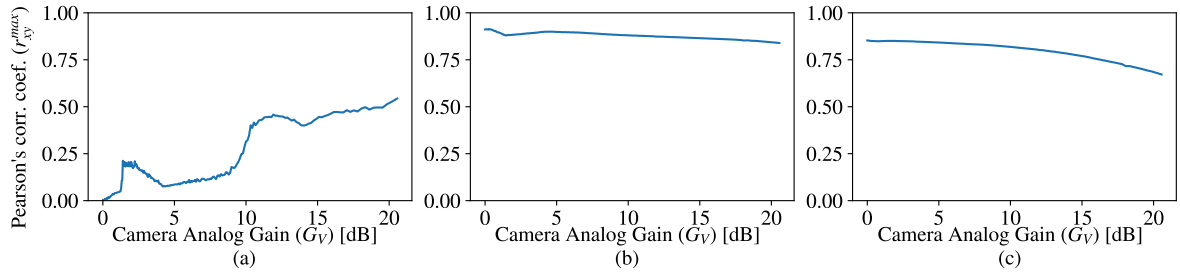


Fig. 5. Data acquisition average values of  $r_{xy}^{max}$  obtained varying  $G_V$  over all the available values. Results from Experiment 1 are shown in (a), Experiment 2 in (b), and Experiment 3 in (c).

TABLE I  
Experiment key parameters.

Parameter	Value
	Transmitter
Device	12 V DC RGB LED strips
Front-end device	Atmel ATmega328p controller [11]
Power levels [W]	min = 1.8, max = 4.8
Dominant wavelengths [nm]	630 (Red), 530 (Green), 475 (Blue)
$T_{chip}$ [s]	1/3600
	Receiver
Camera	Picamera V2 module (Sony IMX219) [10]
Resolution	3280 × 2464 px
$t_{exp}$ [ $\mu$ s]	300
Gain ( $G_V$ ) [dB]	0, ..., 20.6 (233 values)

TABLE II  
Experiments conditions.

	$I$ [ $\mu$ W/cm <sup>2</sup> ]	Gains [dB]	No. of Captures
Experiment 1	3.39	0 - 20.6	50 per each $G_V$
Experiment 2	11.79	0 - 20.6	50 per each $G_V$
Experiment 3	45.11	0 - 20.6	50 per each $G_V$

Where  $r_{xy}^{max(\infty)}$  is the final value after convergence, and  $\epsilon$  is the threshold's parameter (which was set 0.05 arbitrarily for all experiments). The parameter  $r_{th}$  is the final threshold value of the correlation.

## V. RESULTS AND DISCUSSION

The first step of experimentation consisted on the acquisition of frames at all the available  $G_V$  values, and under three conditions of received intensity of radiant energy ( $I$ ), as it is shown in Table II. Each of the three experiment's 11,650 frames were processed to get the Pearson's correlation coefficient with respect to a template signal equal to the transmitted pulses of OOK.

In Fig. 5, the average results of  $r_{xy}^{max}$  obtained from data acquisition and correlation processing are shown for the three experiments. The lowest received intensity of radiant energy at Experiment 1 shows more fluctuations of the correlation,

and it shows that the contribution of  $G_V$  is to improve the signal quality since it is weak. In the other two experiments, a similar behaviour is seen. The high intensity of the received signal makes the gain to deteriorate the signal with saturation, which builds up mostly smoothly. In Experiments 2 and 3, the gain control algorithm should converge to the minimum gain values, and in the Experiment 1, it should converge to the maximum gain. It could also wrongly converge to the local maximum points at 2 dB and 12 dB.

By setting arbitrary initial  $G_V$  values, the correlation data sets evaluated from Experiments 1, 2 and 3 were used to run the gain control algorithm for a fixed number of 150 iterations. In Fig. 6, the results of the chosen  $G_V$  at each iteration are shown. It can be seen that the Experiments 2 and 3 converge to the minimum gain, as expected, in which the correlation is the maximum. The convergence is obtained after about 25 iterations. For the case of Experiment 1, the algorithm takes longer to converge, after about 60 iterations.

The results obtained show that the gain control algorithm can successfully converge to the gain value that ensures maximum correlation available in each scenario. Considering a standard frame rate of 30 fps, and negligible delays at the DSP, the algorithm could converge in about 1 s.

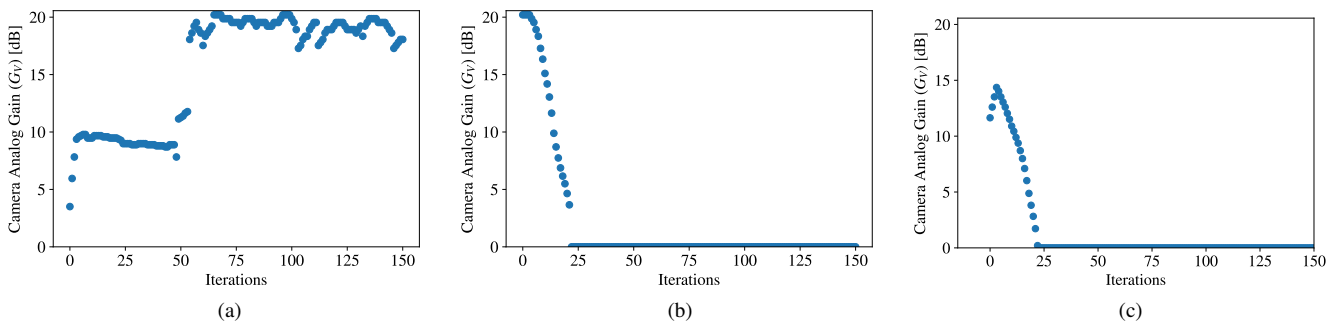


Fig. 6. Convergence of the algorithm in each of the experiments, where (a) corresponds to Experiment 1, (b) to Experiment 2, and (c) to Experiment 3.

## VI. CONCLUSIONS

This work develops an algorithm for the automated control of analog gain in a CMOS sensor camera used in RS-based OCC. It was shown that the camera analog amplifier stage before the ADC can reduce the relative impact of the quantization noise until the received signal is not saturated. In addition, the use of Pearson's correlation coefficient was shown to be an estimator of the signal quality of an image frame captured by the camera, as an alternative to the calculation of SNR. The algorithm was developed for the use of  $r_{xy}$  as the feedback, allowing to estimate the next capture's  $G_V$  to maximize the quality. It was found that in high received power cases, the algorithm converges to the optimal gain in about 25 iterations, whereas in low received power cases, it takes more than double the amount of iterations. With these values, and considering a standard 30 fps frame rate of the camera, the convergence time is between 1 and 2 s. The optimal gain value would be set and the following captures done with the same value. In case of mobility or changing atmospheric conditions, the optical density variations may change the optimal  $G_V$ , making the algorithm necessary to be ran repeatedly. For future work, the experimental setup should be extended to the variation of link span and the attenuation factor by emulated weather conditions, for the parameters of the control algorithm such as damping coefficient and gain seed to be optimized in more realistic conditions.

## REFERENCES

- [1] W. A. Cahyadi, Y. H. Kim, Y. H. Chung, and C. Ahn, "Mobile phone camera-based indoor visible light communications with rotation compensation," *IEEE Photonics Journal*, vol. 8, no. 2, pp. 1–8, April 2016.
- [2] T. Nguyen, Chang Hyun Hong, Nam Tuan Le, and Y. M. Jang, "High-speed asynchronous optical camera communication using led and rolling shutter camera," in *2015 Seventh International Conference on Ubiquitous and Future Networks*, July 2015, pp. 214–219.
- [3] R. Boubezari, H. Le Minh, Z. Ghassemlooy, and A. Bouridane, "Smart-phone camera based visible light communication," *Journal of Lightwave Technology*, vol. 34, no. 17, pp. 4121–4127, Sep. 2016.
- [4] T. Nguyen, A. Islam, T. Hossan, and Y. M. Jang, "Current status and performance analysis of optical camera communication technologies for 5g networks," *IEEE Access*, vol. 5, pp. 4574–4594, 2017.
- [5] A. Islam, M. T. Hossan, and Y. M. Jang, "Convolutional neural networkscheme-based optical camera communication system for intelligent internet of vehicles," *International Journal of Distributed Sensor Networks*, vol. 14, no. 4, p. 1550147718770153, 2018.
- [6] C. Jurado-Verdu, V. Matus, J. Rabadan, V. Guerra, and R. Perez-Jimenez, "Correlation-based receiver for optical camera communications," *Opt. Express*, vol. 27, no. 14, pp. 19 150–19 155, Jul 2019.
- [7] P. Chavez-Burbano, V. Guerra, J. Rabadan, D. Rodríguez-Esparragón, and R. Perez-Jimenez, "Experimental characterization of close-emitter interference in an optical camera communication system," *Sensors*, vol. 17, no. 7, p. 1561, Jul 2017.
- [8] T. Kuroda, *Essential Principles of Image Sensors*. CRC Press, 2017.
- [9] V. Matus, E. Eso, S. R. Teli, R. Perez-Jimenez, and S. Zvanovec, "Experimentally derived feasibility of optical camera communications under turbulence and fog conditions," *Sensors*, vol. 20, no. 3, p. 757, Jan 2020.
- [10] Sony Corporation, *IMX219PQH5-C, Diagonal 4.60 mm (Type 1/4.0) 8 Mega-Pixel CMOS Image Sensor with Square Pixel for Color Cameras, Datasheet*. Sony Corporation, 2014.
- [11] Atmel Corporation, *ATmega328p, 8-bit AVR Microcontroller with 32K Bytes In-System Programmable Flash, Datasheet*. Atmel Corporation, 2015.